JOURNAL OF PETROLEUM GEOMECHANICS
(JPG)

Original article

Developing New Empirical Relations among Strength and Elastic Properties of Carbonate Rocks with Their Petrophysical Properties Using Particle Swarm Optimization Algorithm and Regression Analysis: A Gas Reservoir from Southern of Iran

Amin Asgari[1*], Mohammad Mehrad[2], Imandokht Mostafavi[3], Misha Pezeshki[3]

1- Shahrood University of Technology & MASNA Co. Tehran, Iran
2- Shahrood University of Technology, Shahroud, Iran
3- Pars Oil and Gas Company

Received: 13 June 2024; Accepted: 27 February 2025

DOI: 10.22107/jpg.2025.462735.1235

Keywords

Young's modulus,
UCS,
Carbonate Reservoir,
PSO Algorithm

Abstract

The static Young's modulus (Esta) and the uniaxial compressive strength (UCS) are key parameters in the geomechanical study of hydrocarbon reservoirs. These parameters are typically estimated using empirical models that relate the strength and elastic parameters of the rock to their petrophysical properties. In the present research, the existing empirical models in the literature (specifically for carbonate rocks) were compiled and investigated, this was followed by performing experimental tests on 27 core samples to measure the porosity (n), the density (ρ), the compressive and shear wave velocities (Vp and Vs, respectively), Esta and UCS for a carbonate gas reservoir in the south of Iran. Next, particle swarm optimization (PSO) and regression analysis (RA) were conducted to develop estimator models for the Esta and UCS. Results of this study showed that the best models produced by the PSO algorithm were more accurate than not only the best models produced by the RA, but also the models proposed by previous researchers by 7% and 48%, respectively, for the Esta and by 10% and 7%, respectively, for the UCS. On this basis, it was strongly recommended to apply the empirical correlations developed through the PSO for more accurate estimation of the studied parameters across the investigated field and similar fields.

1. Introduction

The static Young's modulus (Esta) and the uniaxial compressive strength (UCS) of the intact rock are crucial parameters in geomechanical analysis [1] and have numerous applications in the construction of mechanical earth model (MEM) and rock failure criteria [2, 3]. Being among the strength and elastic properties of rock, respectively, the Esta and UCS can be measured according to ASTM standard codes or the ISRM-recommended methods in the laboratory [4, 5]. However, the required experiments are destructive and both time- and cost-intensive. In addition, adequate number of samples with required condition for performing such tests is not always available. This is especially important for the measurement of Esta and UCS of the formations in the hydrocarbon reservoirs, where the core samples from hydrocarbon wells are highly limited in number and costly to retrieve. Accordingly, engineers have been searching for rapid and cost-effective methods for estimating the values of Esta and UCS at minimum possible error. Additionally, the mechanical and strength properties of the rocks are highly variable, being largely dependent on the amount and distribution of porosity, cementation degree, and the particle size and shape [6]. Consequently, establishing a unique relationship between static and dynamic parameters of rocks is extremely challenging. In this respect, data analysis methods have been used to identify robust associations to relate the Esta and UCS values of a rock to the physical properties of the rock.

Given the abovementioned circumstances, numerous research works have been performed to estimate the values of Esta and UCS using low-cost and widely

available data, such as the data obtained upon measuring the physical parameters of a rock (density and porosity), non-destructive ultrasonic tests (Vs and Vp) and the dynamic moduli of the rock (Edyn, υ_{dyn}), leading to the presentation of many relations for various types of igneous, metamorphic, and sedimentary rocks using different data analysis methods including the regression analysis (RA), intelligent algorithms, etc. for fields in different regions [7, 8]. Regarding sedimentary rocks, the estimator relations for the Esta and UCS have been mainly developed for three classes of rocks, namely sandstones, shales, and, in particular, carbonate rocks [9].

Carbonate formations are responsible for more than 60% of the hydrocarbon reservoirs around the world [3, 10, 11] .In addition, the largest oilfields in the world have been formed within the carbonate formations [12]. Accordingly, many efforts have been made to develop estimator relations for the Esta and UCS in the carbonate formations, and this topic has been regarded by the research even more during the recent past (see for example [2, 3, 6, 9, 12-22].

Compared to other sedimentary formations, the carbonate rocks usually come with higher degrees of heterogeneity and structural complexity [11, 12, 20] ، so that the characteristics and behaviors of the carbonate formations are highly variable not only from one formation to another, but also within a single formation [12]. Therefore, the relations developed for estimating the strength and elastic properties (Esta and UCS) of a carbonate rock are usually specific to that particular rock unit, and it is usually not possible to use the relations that were originally developed for a particular formation to estimate the values of Esta and UCS in another formation.

An investigation into the studies performed on the estimator models for the Esta shows that such models have been based on five parameters, namely the porosity (n), the density (ρ), the compressive and shear wave velocities (Vp and Vs, respectively), and the dynamic Young's modulus (Edyn). When it comes to the UCS, in addition to the mentioned five parameters, the static Young's modulus (Esta) has been also taken into consideration.

The majority of the models developed so far have been based on four parameters, namely n, ρ, Vp, and Vs. This has been because of the ease of measuring such parameters in the laboratory using non-destructive tests (NDT) and availability of the corresponding logs to the four parameters for most of the wells drilled into oil and gas fields. Accordingly, the static Young's modulus and uniaxial compressive strength of the corresponding formation along the well can be estimated once their association with one or more of the four parameters was identified. In the meantime, several remarks must be considered before developing/applying such correlations, which are less regarded in the existing literature:

The rock porosity can be measured with a number of different methods. In the relationships developed for carbonate rocks, for example, the porosity has been measured through different methods, including the water absorption method [3, 14, 15], mercury injection [17] and helium injection. The differences among these methods might affect the accuracy of the developed model.

Knowing that the mentioned models are frequently developed based on data-driven methodologies; accuracy of the model outputs has contributions from the amount of available data. In this respect, a larger volume of data implies that a more accurate and generalizable model can be achieved. Lack of access to adequate number of cores for study represents a super challenge in the research works in the field of the oil industry, strongly limiting the number of estimators for Esta and UCS.

The artificial intelligence (AI) and regression analysis (RA) methods have been the most frequently approaches toward the development of estimator methods for the Esta and UCS. The available volume of data acts as a factor that contributes to the choice of the methodology for model development. In this respect, the AI algorithms (e.g. neural networks) require larger volumes of data, as compared to the stochastic methods such as RA. For example, although there is no mathematical relationship to evaluate the minimum required volume of data for achieving an adequately accurate and reliable model based on the structure of a multilayer perceptron (MLP) neural network (NN), but a rule of thumb indicates that the volume of the data must be at least 10 times as large as the number of unknowns (sum of weights and biases) of the network. A review of the previous works shows that this data adequacy has been widely ignored in some studies.

A study on the developed models for carbonate rocks shows that most of these equations are based on the experiments performed on the specimens taken from the exposed outcrops (Appendix I). Accordingly, application of the equations developed based on the results of the tests performed on surface samples for estimating the values of Esta and UCS of a deeply buried reservoir formation may end up with significant errors due to the remarkable differences in the stress history, involved fluids, and coring conditions, which could have acted to change the mechanical behavior of the rock.

In this study, laboratory-measured physical properties (n, ρ, Vp and Vs) of the samples taken from two wells drilled into a carbonate formation in a gasfield in the

south of Iran were used to develop an estimator model for the Esta and UCS. For this purpose, we began with compiling similar correlations proposed by previous researchers and evaluating their accuracies for estimating the Esta and UCS values on the studied samples. Next, based on the available data, the particle swarm optimization (PSO) and linear and nonlinear bivariate regression analysis (BRA) were used to develop estimator models, with their results then compared to one another.

2. Sample preparation and experimental procedure

2-1. Sample selection and preparation

The studied interval represented the reservoir horizon in a gasfield in the south of Iran near the Persian Gulf. Geologically, the Kangan and Dalan Formations were the main constituents of the gasfield [23]. Comprising a total thickness of about 450 m, the Kangan and Dalan Formations are mainly composed of limestone and dolomite with anhydrate interbeddings. Accordingly, for the sake of the present research, a total of 27 core samples taken from two wells drilled into this field were considered. Of the pool of 27 core samples, 12 core samples were retrieved from the first well, with the remaining 15 cores taken from the second well. Macroscopic and microscopic evaluations of the core samples showed that, in terms of texture, those were composed of limestone and dolomite crystals with grains of ooids, oncoids, and intra-clastic particles, though anhydrate cements have been also observed on some samples [24]. Figure 1 demonstrates the images of CT scans, microscopic analysis, and typic thin sections of the collected rock samples from the studied reservoir interval. The CT scan images were used to not only determine the rock type, but also to check for the presence of the cracks and fractures in the samples.

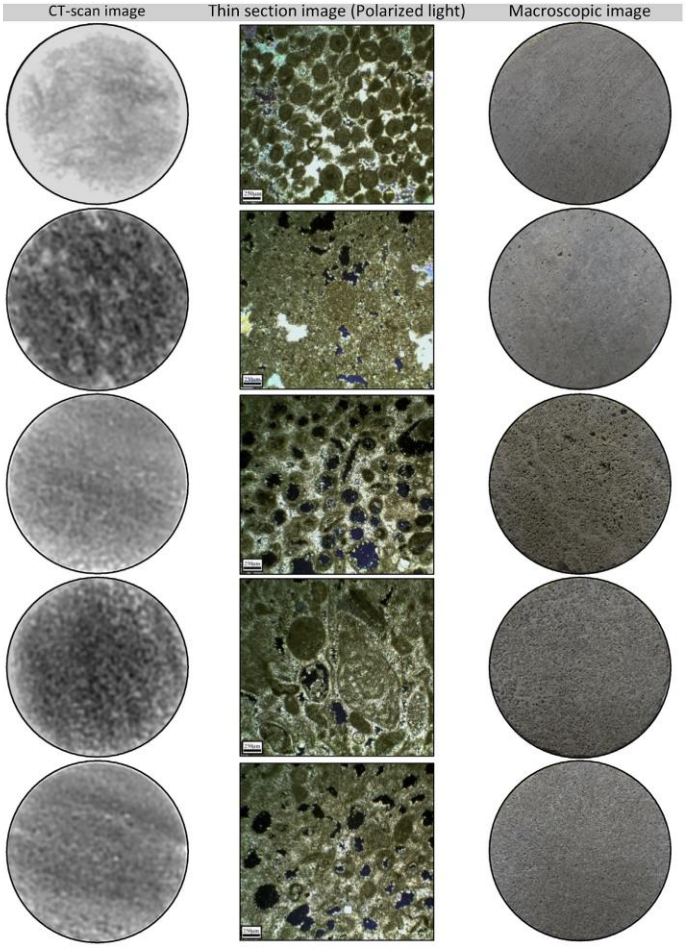

Fig 1. Images of CT scan, microscopic analysis, and typic thin sections of the studied samples[۲۴]

2-2. Experimental procedure

Nondestructive measurements were performed on all samples to evaluate the required parameters, including the density (through dimensional measurement), porosity (through gaseous helium injection), and Vp and Vs at room temperature. Figure 2 shows the experimental setup used to determine the ultrasonic wave velocity in this study. Subsequently, the samples were subject to UCS tests where radial and axial strains were further measured (Figure 3). The static Young's modulus (Esta) was measured based on the secant modulus at 50% UCS (i.e. Es(50)) [4]. Table 1 provides the statistical evaluation of the results of the measurements experiments performed on the 27 core samples based on lithology. It is worth noting that the values of the dynamic Young's modulus in this table were calculated from Equation (1).

$$E_{dyn} = \rho V_s^2 \times \left(\frac{3V_P^2 - 4V_s^2}{V_P^2 - V_s^2}\right) \qquad 1$$

Fig 2. Experimental apparatus for ultrasonic wave velocity measurement.

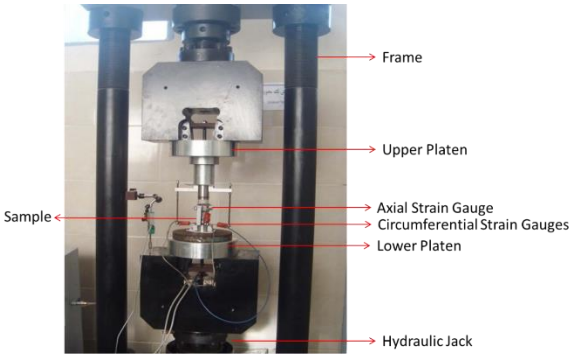

Fig 3. Configuration of the uniaxial testing apparatus for measuring the UCS and Esta.

Table 1. Statistical evaluation of the physical, elastic, and strength parameters including density, porosity, compressive and shear wave velocities, UCS, Esta and dynamic Young's modulus (Edyn) based on lithology.

	Lithology							
	Dolomite				Limestone			
Number of samples	12				15			
Statistical indicators	Min	Max	Average	Standard Deviation	Min	Max	Average	Standard Deviation
ρ (g/cc)	1.94	2.84	2.32	0.36	2.04	2.80	2.40	0.25
n (%)	1.16	28.62	17.13	10.68	1.74	24.83	13.35	7.67
Vp (km/s)	2.88	5.14	3.75	0.86	3.01	4.80	3.78	0.59
VS (km/s)	1.65	2.91	2.19	0.49	1.59	2.71	2.17	0.41
ESta (Gpa)	6.05	62.92	23.00	22.84	4.88	39.94	20.78	12.19
UCS (Mpa)	10.15	167.13	53.81	55.87	14.98	136.33	55.70	39.87
Edyn (GPa)	13.48	60.56	30.53	18.63	13.71	47.82	29.92	12.59

3. Evaluation of the existing empirical correlations

Previous researchers have proposed numerous correlations for estimating the Esta and UCS in the carbonate rocks. This section evaluates the efficiency and accuracy of these correlations for estimating the Esta and UCS on the samples considered in this study. For this purpose, based on a review of the relevant literature, all of the estimator correlations developed for the Esta and UCS based on the porosity, density, compressive and shear wave velocities, and static and dynamic Young's modulus in the carbonate rocks were extracted and classified. The correlations were then evaluated based on the values of the root-mean-square error (RMSE) (Equation 2) and correlation

coefficient, R2 (Equation 3) for the experimental results obtained in the present study.

$$R^2 = \frac{N\sum xy - \sum x \sum y}{\sqrt{[N\sum x^2 - (\sum x)^2][N\sum y^2 - (\sum y)^2]}} \quad 2$$

$$RMSE = \sqrt{\sum_{i=1}^{N} \frac{(x_i - y_i)^2}{N}} \quad 3$$

In the abovementioned relationships, the R2 and RMSE were calculated for N pairs of data points from the predicted (x) and measured (y) values.

Tables 9 and 10 Appendix I provide a complete set of the results of all of the compiled correlations for predicting the Esta and UCS, respectively. Among the entire pool of the correlations evaluated in this study, the best estimators of the Esta and UCS – indicated by the minimum RMSE considering the type and combination of the input parameters – are listed in Tables 2 and 3, where the correlations are sorted in an increasing order of RMSE. These tables were established for cases where the researcher has access to a particular rock property and seeks for the best estimation based on that available parameter. Although the value of RMSE must be interpreted in proportion to the scale of changes in other parameters, but as observed in the tables, the correlations presented for the static Young's modulus exhibited generally lower RMSE values than those proposed for the UCS.

Among the best correlations for estimating the Esta, as listed in Table 2, the one proposed by [25] was found to be the most accurate. This indicates that one may obtain more accurate estimations of the static Young's modulus by considering the dynamic Young's modulus in the same field. Qualitative investigation of the top model in Figure 4a shows that the model underestimated the Esta significantly.

Investigation of the best models for estimating the UCS based on the data presented in this research (as detailed in Table 3) shows that the correlation proposed by [26] outperformed the other correlations by adopting a merely single-parameter (i.e. the porosity) equation. This implied that, for the data encountered in the present study, one can achieve an empirical model of higher accuracy by focusing on the porosity rather than the other parameters. Qualitative assessment of this model in Figure 4b shows that the model tended to overestimate the UCS values lower than 40 MPa while underestimating the ones above 70 MPa.

A very interesting point to note about the considered model was the higher accuracy of the single-parameter models rather than those that were developed based on a combination of multiple input parameters for estimating the Esta and UCS. Accordingly, it seems that the models developed on the basis of two or more parameters were more accurate than their single-parameter counterparts for the specific field for which those were developed, but rather provided limited generalizability compared to the single-parameter models.

Table 2. The best empirical correlations for estimating the E_{sta} based on the data from the studied field, separated by the type and combination of the input parameters used to develop the model (ranked by RMSE).

Input parameter(s)	Equation	RMSE (GPa)	R-squared	Researcher (Year)
$\boldsymbol{E_{dyn}}$	$E_{sta} = 1.153E_{dyn} - 15.2$	3.12	0.86	[25]
$\boldsymbol{n}$	$E_{sta} = 69 - 19.3 \ln(n)$	5.89	0.89	[24]
$\boldsymbol{V_p}$	$E_{sta} = 0.169V_p^{3.324}$	9.81	0.94	[6]
$\boldsymbol{\rho, n, V_p, V_s}$	$E_{sta} = -23.689 + 2.99\rho - 0.36n + 19.835V_p - 19V_s$	13.48	0.89	[27]
$\boldsymbol{\rho, E_d}$	$E_{sta} = 10^{(0.02+0.7\log(\rho E_{dyn}))}$	20.53	0.94	[28]
$\boldsymbol{\rho}$	$E_{sta} = 3.98 \times e^{5.238\rho}$	23.65	0.86	[29]
$\boldsymbol{\rho, n, V_p}$	$E_{sta} = 76.534 - 2.709\rho + 0.271n - 11V_p$	29.52	0.93	[30]

E_{sta}: (GPa), E_{dyn}: (GPa), Vp: (km/s), Vs: (km/s), $\boldsymbol{\rho}$: (g/cc), n: (%)

Table 3. The best empirical correlations for estimating the UCS based on the data from the studied field, separated by the type and combination of the input parameters used to develop the model (ranked by RMSE).

Input parameter(s)	Equation	RMSE (MPa)	R^2	Ref.
n	$UCS = 147.16 \times e^{-0.0835n}$	15.15	0.90	[26]
E_{dyn}	$UCS = 12.8 \times (E_{dyn}/10)^{1.32}$	18.02	0.86	[6]
E_{sta}	$UCS = 2.27E_{sta} + 4.74$	17.77	0.86	[31]
E_{sta}, n	$UCS = 2.94 \times E_{sta}{}^{0.834}/n^{0.088}$	19.35	0.87	[32]
V_p	$UCS = e^{0.99V_p}$	23.49	0.74	[33]
ρ	$UCS = 70.74\,\rho_{dry} - 116.26$	29.27	0.79	[34]
E_{sta}	$UCS = 25.1 \times E_{sta}{}^{0.34}$	32.15	0.84	[35]
V_p, ρ	$UCS = 142.47 \times e^{-9.561/(\rho V_p)}$	33.75	0.80	[36]
ρ, n, V_p	$UCS = -92.305 + 33.66\rho - 0.61n + 12.27V_p + 3V_s$	35.10	0.83	[27]

UCS: (MPa), Esta: (GPa), Edyn: (GPa) Vp: (km/s), Vs: (km/s), ρ: (g/cc), n: (%)

4. Estimator model development tools

Knowing that AI-based methods (i.e. NNs) required huge amounts of data to produce reliable results while the experimental data on only 27 core samples was available in the present work, the use of AI methods was infeasible for this work. Accordingly, regarding the widespread success of the evolutionary optimization algorithms in the engineering problems for determining optimal coefficients of empirical models and the pervasive application of the RA, such algorithms were used for the development of empirical estimators for the Esta and UCS. Each of these algorithms is briefly described in the following.

4-1. PSO algorithm

Proposed by [37], the PSO is an evolutionary collective intelligence-based algorithm that simulates the hunting behaviors of the fishes or birds. Thanks to its simple understandable structure, this algorithm has drawn many researchers' attention. In the field of petroleum geomechanics, the PSO has been frequently applied as learning algorithm for NNs and adaptive neuro-fuzzy inference systems (ANFIS) or to determine constants of the empirical models [38, 39].

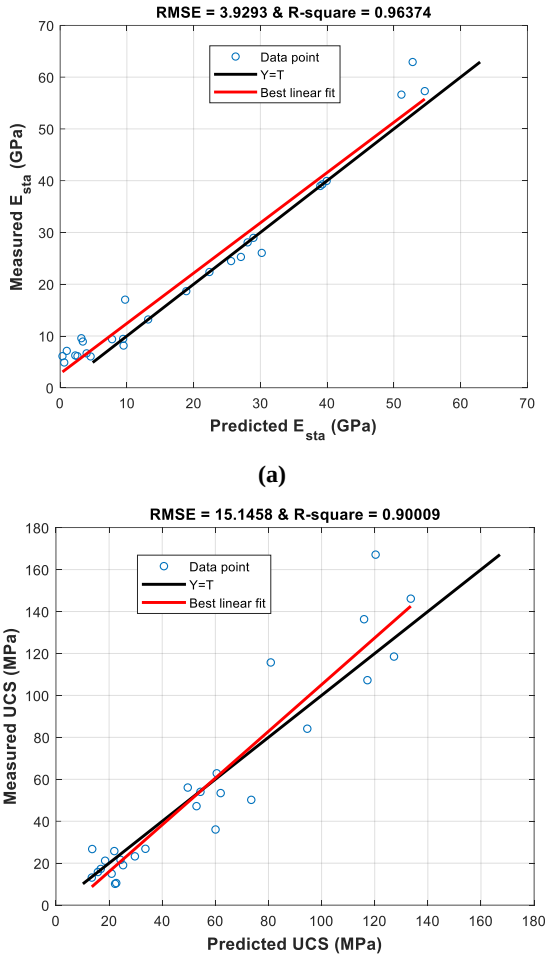

Fig 4. Cross plots of (a) measured-versus-estimated static Young's modulus using the Nur and Wang, 2000 model, and (b) measured-versus-estimated UCS using the Kılıç and Teymen, 2008 model.

In this algorithm, each particle possesses two properties, namely a position (x) and a velocity (V), with the position being a desirable solution for the optimization problem in the search space. Firstly, the position and velocity of each cell are set on a random basis while maintaining the constraints applied to the particles. The set position for each particle is stored as its best personal position (Pb). Subsequently, the objective function is used to evaluate the position of every single particle, and the particle for which the objective function returns the minimum value is

selected as the best position of the particle generation (Gb). At each iteration, a new velocity (Vi (t + 1)) is updated dynamically for each particle (i) with reference to its previous velocity (Vi (t)) and the distance between its current position (xi (t)) from the best personal position and the best position of the particle generation (Equation 4). The new position of each particle is then updated based on its previous position and the updated velocity (Equation 5). Subsequently, the new position of the particle is evaluated through the objective function and the best personal and generation positions are updated by comparing the new values of the objective function with the previous best personal and generation positions. This iterative process is continued until the "stoping criterion" is met [40-44].

$$V_i(t+1) = wV_i(t) + c_1 r_1\left(Pb_i(t) - x_i(t)\right) + c_2 r_2(G_b(t) - x_i(t)) \quad 4$$

$$x_i(t+1) = x_i(t) + V_i(t+1) \quad 5$$

here i = 1, 2, …, n with n being the number of particles in the swarm, w is the inertial weight (the recurrence rate controls the particle velocity [45], c1 and c2 are positive coefficients called personal and collective learning coefficients, respectively, and r1 and r2 are random numbers in the range of [0, 1] [46].

4-2. Regression analysis

In the statistics, the process through which a correlation is developed between a dependent variable and one or more independent variables is known as the regression analysis (RA), and the models developed in this way are called regression models. A regression model linking some independent variables to a dependent variable can be either linear or nonlinear. Equation (6) expresses the mechanism through which a dependent variable Y is calculated from the independent variable X via linear RA.

$$Y = \alpha + \beta X + \varepsilon \quad 6$$

In this equation, α and β are the intercept and slope of the fitted line, respectively, and ε is the deviation between the observed and estimated values of Y – termed as residual. In the linear RA, the objective is to find the values of α and β in Equation (7) in such a way to minimize the residual sum of squares (RSS) over the entire set of data (n data points), as expressed by Equation (8). In the statistics, this methodology is known as least squares method, for which two assumptions are considered [47]: (1) the relation between X and Y represents a straight line, and (2) the residuals are independent and exhibit a normal distribution with a variance of σ2 around a mean value of 0.

$$\hat{Y} = \alpha + \beta X \quad 7$$

$$RSS = \sum_{i=1}^{n} \varepsilon_i^2 \quad 8$$

The least square method has been also applied in the nonlinear models, but its mechanism of action is slightly different depending on whether the nonlinear model can or cannot be converted to a linear model.

5. Results and discussion

Investigation of the variation of the dependent variable with different independent variables in the form of scatter plots – before applying the estimator tools – can largely help determine the most effective parameters and appropriate model to relate them. Figure 5 presents the scatter plots of the porosity, density, compressive and shear wave velocities, and the dynamic Young's modulus, as independent variables, against the laboratory-measured static (secant) Young's modulus, as the dependent variable. As observed on this figure, it seems that the independent variables were exponentially related to the static Young's modulus, though the effect of the dynamic Young's modulus on the static Young's modulus could be well represented by a linear equation. Except for the porosity, which exhibited an inverse association with the static Young's modulus, the other parameters shown in Figure 5 were found to be directly related to the static Young's modulus, so that the modulus increased with increasing the mentioned parameters.

Figure 6 demonstrates the scatter plots of the porosity, density, compressive and shear wave velocities, and the dynamic Young's modulus against the UCS values measured in the laboratory. The figure implies that relationship between each of the independent variables and the UCS were governed by a nonlinear exponential equation, though here again a seemingly linear relation was observed between the static and dynamic Young's moduli, in one hand, and the UCS, on the other hand. This figure clearly indicates that all of the considered parameters were directly correlated to the UCS, except for the porosity, which exhibited an inverse association with the UCS.

Although the assessments performed so far revealed the models governing the inter-parameter relations partly, yet accurate determination of the governing model required the application of estimator tools. Accordingly, application of the PSO and RA for the development of empirical models for estimating the static Young's modulus and UCS is discussed in the following.

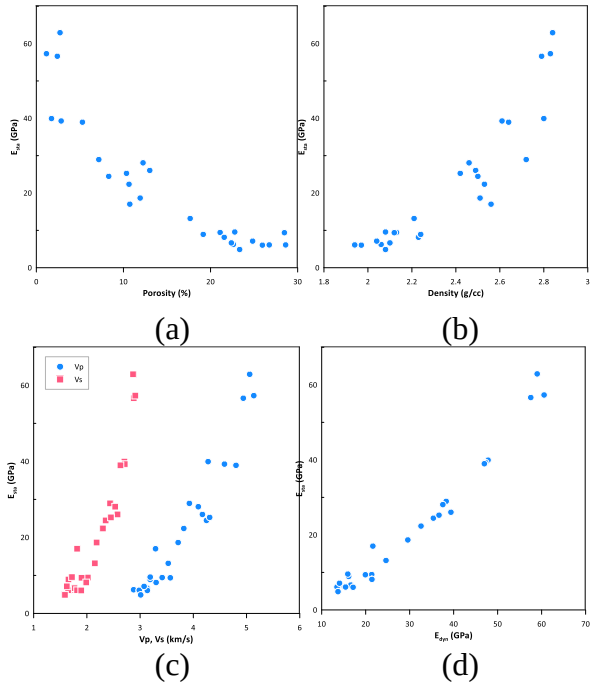

Fig 5. The relations between (a) porosity, (b) density, (c) compressive and shear wave velocities, and (d) dynamic Young's modulus, in one hand, and the laboratory-measured static Young's modulus, on the other hand.

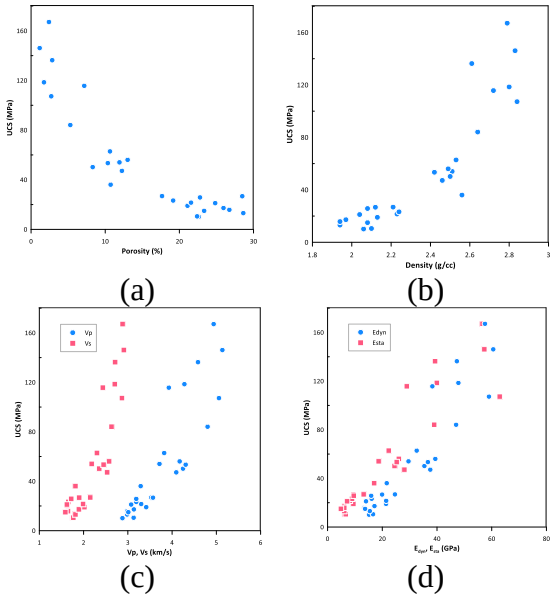

Fig 6. The relations between (a) porosity, (b) density, (c) compressive and shear wave velocities, and (d) dynamic and static Young's moduli, in one hand, and the laboratory-measured UCS, on the other hand.

5-1. Development of empirical correlations using the PSO algorithm

In order to utilize the PSO algorithm for developing estimator models, the basic forms of the empirical equations presented in the literature on the Esta and UCS were identified. Presented in Table 4, these basic forms were composed of a number of constant coefficients (c (i)) and input parameters (IP (i)). The output parameter (OP) of these basic forms was either the Esta or the UCS. Given that the IPs and Ops were known – as those were actually measured in the laboratory – the PSO algorithm was run in an attempt to determine the values of the constant coefficients optimally. The constant coefficients served as the decision variables in the PSO; i.e. those had to be determined in such a way to minimize the RMSE of the model. Following a trial-and-error approach, the maximum number of constant coefficients included in these basic forms was set to 100. Trying to identify the optimal number of particles, it was found that the algorithm would converge to a solution in less than 300 iterations. Accordingly, the maximum allowable number of iterations was set to 300.

To ensure physically meaningful solutions and prevent unrealistic parameter estimations, constraints were incorporated into the optimization process. Specifically, upper and lower bounds were imposed on the constant coefficients to restrict them within a reasonable range based on prior knowledge and empirical correlations. These bounds prevented the algorithm from exploring infeasible regions in the search space, improving solution stability. Additionally, a penalty strategy was employed to handle constraint violations. If a particle moved beyond the predefined bounds, its objective function was assigned an infinite value, effectively eliminating infeasible solutions from further consideration. This ensured that the PSO prioritized feasible solutions while maintaining exploration capabilities.

Table 4. The basic forms identified by investigating the existing empirical correlations for estimating the values of Esta and UCS and applied constraints on the coefficients.

Basic form	Number of input(s)	Number of coefficients	Constraints
$OP = c(1) \times IP(i) + c(2)$	1	2	**0.00001 < c(1) <1000 -300 < c(2), c(3) and c(4) <300**
$OP = c(1) \times e^{c(2)\times IP(i)}$	1	2	
$OP = c(1) \times IP(i)^{c(2)}$	1	2	
$OP = c(1) \times e^{c(2)\times IP(i)^{c(3)} IP(j)^{c(4)}}$	2	4	
$OP = c(1) \times IP(k) \times e^{c(3)\times IP(i)^{c(4)} IP(j)^{c(5)}}$	3	5	

Table 11 (Appendix II) provides a list of the PSO-derived estimator models for Esta based on the data

considered in this study, with the models classified based on the type of the IP and the core function. Among these models, the best ones are tabulated in Table 5, where the models are classified by the IP. As indicated in Table 5, one could utilize an exponential equation to estimate the static Young's modulus from the dynamic Young's modulus at high accuracy. This correlation provided significantly higher accuracy in estimating the Esta, as compared to the one proposed by [25]. On the other hand, investigation of the cross plot of the measured values of Esta versus the estimations produced by the best model derived via the PSO (Figure 7a) showed that the best fitted line ended up laying on Y = T, showing that the developed model was neither systematically overestimating nor underestimating the actual values. Variations of error through successive iterations of the PSO algorithm when attempting to develop the model are demonstrated in Figure 7b. As indicated on this figure, the algorithm converged to an optimal solution in less than 100 iterations.

Table 5. The best models developed, using the PSO, for estimating the Esta based on the studied data.

Input parameter	Equation	RMSE (GPa)	R^2
E_{dyn}	$E_{sta} = 0.0691E_{dyn}^{1.6505}$	2.11	0.98
V_s	$E_{sta} = 0.3098e^{1.8103V_s}$	3.30	0.96
V_p	$E_{sta} = 0.0952V_p^{3.9546}$	4.14	0.94
n	$E_{sta} = 61.1913e^{-0.893n}$	5.22	0.91
ρ	$E_{sta} = 0.0332e^{2.6215\rho}$	5.28	0.90

The PSO model was further used to develop estimator models for the UCS based on the data utilized in this work. The relations obtained through this approach are given in Table 12 (Appendix). The model selection (i.e. to select the best models in terms of the type and combination of the IPs) was performed based on the resultant error, with the results presented in Table 6. As observed in this table, among the relations explored in this study, the highest level of accuracy was provided by the exponential model driven by a single IP: the porosity. The associated error with this single-parameter model was significantly lower than that of the multi-variable correlations. A comparison between this best model and the one proposed by [26] – which was known to have outperformed the other UCS predictor models in the literature – showed the superior accuracy of the model developed by the authors in the current study. The cross plot of the measured values of UCS against estimations produced by the best-fitted model derived via the PSO (Figure 8a) showed that the developed model neither systematically overestimated nor underestimated the actual values. An investigation into the evolution of error at different iterations (Figure 8b) showed that this algorithm could achieve to the optimal solution at some iteration around the 60th.

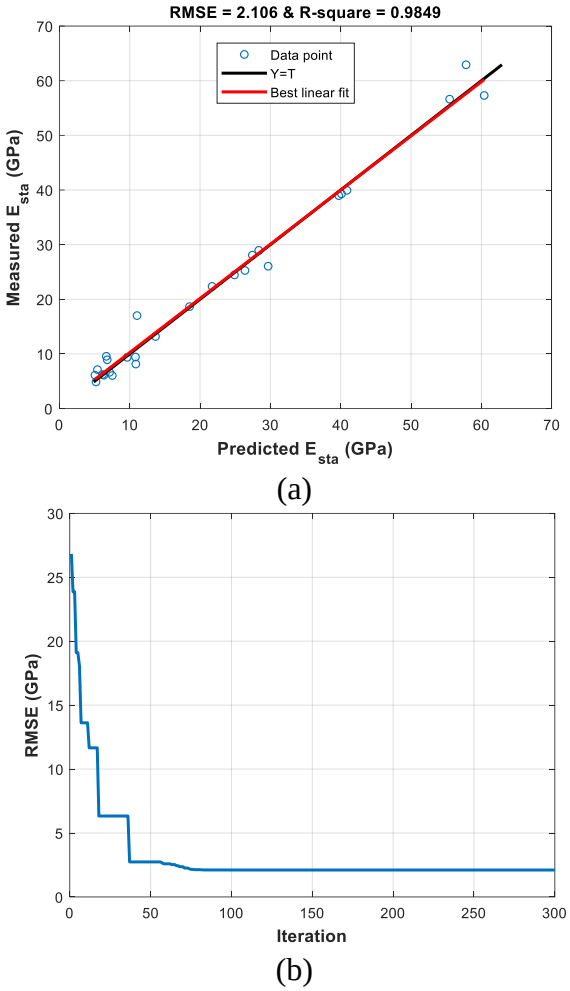

Fig 7. (a) Cross plots of the measured static Young's modulus and the corresponding estimate produced by the best-fitted model using the PSO, and (b) variations of error through successive iterations of the PSO for the best-fitted model.

5-2. Development of empirical equations using the RA

Results of the PSO-derived model for estimating the Esta and UCS were validated through the regression analysis – a popular method for developing empirical correlations in the past, as mentioned in the literature review.

The models built upon applying the RA for estimating the Esta are presented in Table 13 (Appendix II). A comparison between this table with the results of the PSO-derived model for estimating the Esta (Table 11, Appendix II) shows that the two methods produced similar results using the corresponding linear models.

It was while the PSO algorithm outperformed the RA when it came to the nonlinear models. This finding clearly indicated the weakness of the RA for developing nonlinear models. This could be attributed to the sensitivity of the least squares method to non-normality of the data. In addition, the RA method is suitable for modeling the variables that are known to be linearly related to the target variable.

Table 6. The best models developed, using the PSO, for estimating the UCS based on the studied data.

Input parameter (s)	Equation	RMSE (MPa)	R^2
n	$UCS = 164.5985e^{-0.0979n}$	14.11	0.91
V_p, ρ, n	$UCS = 259.9612 \times n^{-0.25} \times e^{-68.7524\rho^{-3.0119}V_p^{-1.1706}}$	14.69	0.90
E_{sta}, n	$UCS = 13.3878 \times {E_{sta}}^{0.6251} / n^{0.2308}$	15.55	0.89
E_{dyn}	$UCS = 0.2111E_{dyn}^{1.6006}$	16.92	0.86
E_{sta}	$UCS = 3.0347E_{sta}^{0.9484}$	17.29	0.86
ρ	$UCS = 0.1218\rho^{6.7751}$	17.33	0.86
V_s	$UCS = 0.8356e^{1.7852V_s}$	17.78	0.85
V_p	$UCS = 58.0776V_p - 164.0326$	21.91	0.77

Table 7 presents a list of the best estimators obtained by the RA for estimating the Esta, with the results sorted based on the minimal estimation error and classified by the IP. According to this table, it is evident that the maximum accuracy was obtained when the Esta was estimated from the Edyn through some exponential equation, as compared to the other models reported in the table. However, this model was still less accurate than the best model built through the PSO. The cross plot of the measured values of the Esta versus estimated values of that by the RA-derived model (Figure 9) shows that the model tended to significantly underestimate the Esta at UCS values beyond 35 MPa. In this respect, the use of this model is not recommended for high UCS values.

The UCS estimator models built through RA based on the studied data in this work are presented in Table 14 (Appendix II). With reference to the associated error, the best equation for each IP was selected from the table and listed in Table 8 for further analysis. As seen on Table 8, the exponential porosity model produced the most accurate estimations of the UCS.

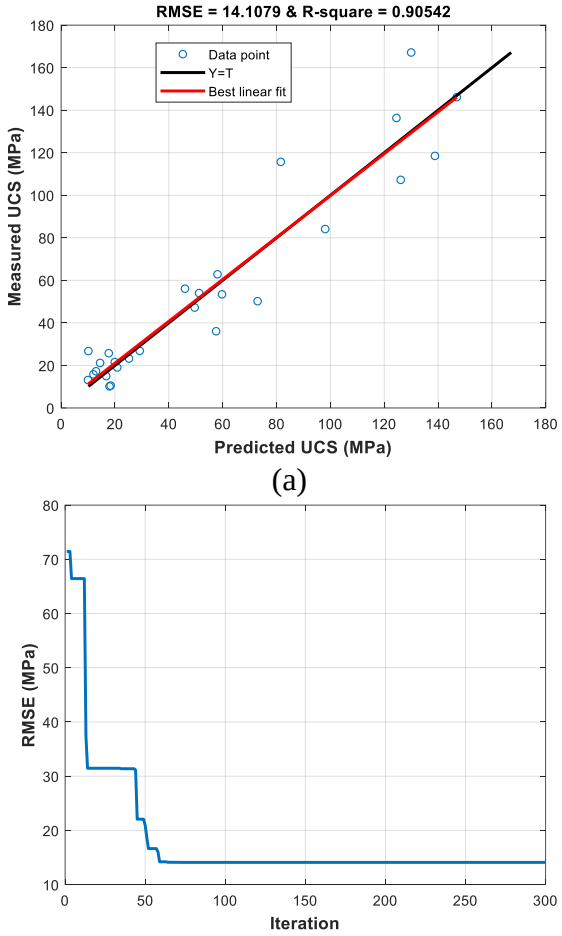

Fig 8. (a) Cross plots of the measured UCS and the corresponding estimates produced by the best-fitted model using the PSO, and (b) variations of error through successive iterations of the PSO for the best-fitted model.

Table 7. The best models developed, using the RA, for estimating the Esta based on the studied data.

Parameter	Equation	RMSE(GPa)	R^2
E_{dyn}	$E_{sta} = 0.0893E_{dyn}^{1.5785}$	2.26	0.96
V_s	$E_{sta} = 0.3372e^{1.7695V_s}$	3.38	0.91
V_p	$E_{sta} = 0.0567V_p^{4.3034}$	4.34	0.93
ρ	$E_{sta} = 0.0339e^{2.6036\rho}$	5.32	0.92
n	$E_{sta} = 57.293e^{-0.085n}$	5.38	0.92

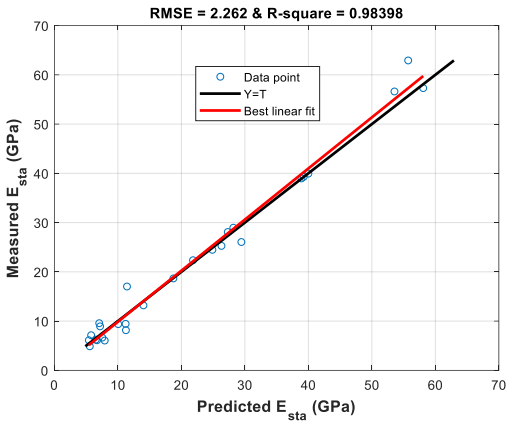

Fig 9. Cross plot of the measured Esta and the corresponding estimates produced by the best-fitted model using the RA.

Although the proposed methodology is focused on developing single-variable models, yet the comparison of such models in terms of the development method (RA or PSO) and the IP showed that different best functions were selected for different development methods with Esta and ρ as IP. Comparison of the error associated with these two methods for estimating the UCS indicated low level of the error for the models developed by the PSO algorithm, as compared to the RA. In addition, qualitative evaluation of the cross plot of the measured and estimated values of UCS from the best model produced by the RA (Figure 10) shows that the model works inappropriately at higher values of UCS, significantly underestimating the actual value of UCS. Accordingly, this model is strictly not recommended for relatively high values of UCS.

Table 8. The best models developed, using the RA, for estimating the UCS based on the studied data.

Parameter	Equation	RMSE (MPa)	R-squared
n	$UCS = 144.27e^{-0.087n}$	15.46	0.87
E_{dyn}	$UCS = 0.2009E_{dyn}^{1.6017}$	17.20	0.88
E_{sta}	$UCS = 2.4845E_{sta} + 0.7796$	17.38	0.86
ρ	$UCS = 0.064e^{2.7093\rho}$	17.75	0.89
V_s	$UCS = 0.7911e^{1.785V_s}$	18.16	0.83
V_p	$UCS = 58.078V_p - 164.03$	21.91	0.77

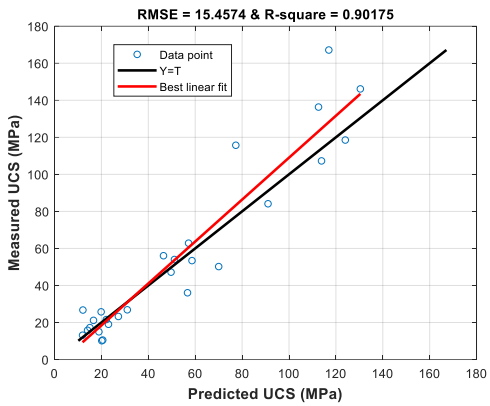

Fig 10. Cross plot of the measured UCS and the corresponding estimates produced by the best-fitted model using the RA.

6. Conclusion

Given the key role played by the geomechanical parameters, especially the uniaxial compressive strength (UCS) and static Young's modulus (Esta) in the determination of the safe mud weight window, drilling bit selection, hydraulic fracturing, ground subsidence, and caprock integrity, the present research was dedicated to the evaluation and development of estimator models for the UCS and Esta. For this purpose, a total of 27 core samples from a carbonate gasfield in the south of Iran were considered. On each sample, the values of the density, porosity, compressive and shear wave velocities, static Young's modulus, and UCS were measured through experimentation.

Application of the 22 estimator models for the Esta, which were compiled from the literature on the carbonate rocks, on the experimental data obtained in this research showed that the empirical model proposed by [25] was more accurate than the other models. Among the pool of 72 empirical models presented in the literature for estimating the UCS of carbonate rocks, the one proposed by [26] was found to be the most accurate for estimating the parameters focused in this work.

Investigation of the variation of different parameters with the static Young's modulus and UCS in the form of scatter plots showed that, except for the porosity, all other parameters were directly related to the Esta and UCS. In addition, evaluations indicated that a nonlinear exponential equation governed the relation between each input parameter (IP) and either Esta or UCS. This was while the results showed that linear relations could better describe the relationship between the dynamic Young's modulus, in one hand, and either of the static Young's modulus and UCS, on the other hand. Accordingly, a greater focus was put on these three types of function for developing estimator models for the Esta and UCS based on single

IP. Modeling the Esta using the particle swarm optimization (PSO) showed that this parameter could be estimated by an exponential function of the dynamic Young's modulus with a minimum root-mean-square error (RMSE) of 2.11 GPa. Comparison of this finding to the reported results of Nur and Wang (2000) and the best model produced by regression analysis (RA) showed the higher accuracy of the PSO-derived model by 48% and 7%, respectively. Utilization of the PSO algorithm for developing a model for estimating the UCS also showed that an exponential function of the porosity could estimate the UCS at a minimum RMSE of 14.11 MPa. Comparing the PSO-derived model with the one presented by Kilic and Teymen (2008) and the best equation developed by the RA confirmed the superiority of PSO as it produced more accurate results by 7% and%, respectively. In addition, a comparison between the single- and multi-IP models produced by the mentioned methodologies showed that the single-IP models tended to offer higher accuracies and further generalizability, as compared to the multi-IP models, though the fundamentals of the rock mechanics indicate that the UCS and static Young's modulus are affected by multiple rock properties. Finally, due to inappropriate performance of the least squares method for the RA-derived models, the RA is not recommended for developing estimator models for the Esta and the UCS.

7. Recommendation for future study

While this study successfully developed and optimized estimator models using the PSO algorithm, several directions for future research can be explored:

Although the dataset used in this study was sufficient for applying the PSO algorithm and developing reliable estimator models, increasing the number of samples could further enhance model robustness and generalization. Future research could focus on expanding the dataset by incorporating additional experimental or field measurements from diverse geological formations. This would allow for a more comprehensive evaluation of the developed models across a wider range of conditions.

Incorporating additional parameters, such as mineralogical composition, pore structure, or anisotropy effects, could improve the accuracy and generalization of the models.

Future studies could explore the integration of PSO with other optimization techniques, such as grey wolf optimizer (GWO), to enhance convergence speed and accuracy.

Advanced machine learning techniques, such as deep neural networks or transformer-based models, could be investigated for their potential to capture complex relationships in rock mechanics data.

Incorporating uncertainty quantification techniques, such as Monte Carlo simulations or Bayesian inference, could help assess the reliability of the predictions and improve confidence in the developed models.

8. Acknowledgement

The authors would like to appreciate the Pars Oil and Gas Company (POGC) for providing the required data and granting the permission to release this article.

9. Conflict of interest

The authors declare there is no conflict of interest.

10. References

[1] Zhang, J.J., Applied Petroleum Geomechanics. 2019: Gulf Professional Publishing**.**

[2] Elkatatny, S., et al., An integrated approach for estimating static Young’s modulus using artificial intelligence tools. Neural Computing and Applications, 2019. 31 **:(**۸**)**p. 4123-4135**.**

[3] Madhubabu, N., et al., Prediction of compressive strength and elastic modulus of carbonate rocks. Measurement, 2016. 88: p. 202-213**.**

[4] ASTM, D7012-14 (2014) Standard test methods for compressive strength and elastic moduli of intact rock core specimens under varying states of stress and temperatures. ASTM International, West Conshohocken, 2014**.**

[5] Ulusay, R., The ISRM suggested methods for rock characterization, testing and monitoring: 2007-2014. 2014: Springer**.**

[6] Najibi, A.R., M. Ghafoori, G.R. Lashkaripour, and M.R. Asef, Empirical relations between strength and static and dynamic elastic properties of Asmari and Sarvak limestones, two main oil reservoirs in Iran. Journal of Petroleum Science and Engineering, 2015. 126: p. 78-82**.**

[7] Briševac, Z., P. Hrženjak, and R. Buljan, Models for estimating uniaxial compressive strength and elastic modulus. Građevinar, 2016. 68(01.): p. 19-28**.**

[8] Deere, D.U. and R. Miller, Engineering classification and index properties for intact rock. 1966, Illinois Univ At Urbana Dept Of Civil Engineering**.**

[9] Chang, C., M.D. Zoback, and A. Khaksar, Empirical relations between rock strength and physical properties in sedimentary rocks. Journal of Petroleum Science and Engineering, 2006. 51(3-4): p. 223-237**.**

[10] Akbar, M., et al., A snapshot of carbonate reservoir evaluation. Oilfield Review, 2000. 12(4): p. 20-21.

[11] Sayers, C.M., The elastic properties of carbonates. The Leading Edge, 2008. 27(8): p. 1020-1024.

[12] Bakhorji, A.M., Laboratory measurements of static and dynamic elastic properties in carbonate. 2010.

[13] Aboutaleb, S., M. Behnia, R. Bagherpour, and B. Bluekian, Using non-destructive tests for estimating uniaxial compressive strength and static Young's modulus of carbonate rocks via some modeling techniques. Bulletin of Engineering Geology and the Environment, 2018. 77(4): p. 1717-1728.

[14] Çelik, S.B., Prediction of uniaxial compressive strength of carbonate rocks from nondestructive tests using multivariate regression and LS-SVM methods. Arabian Journal of Geosciences, 2019. 12(6): p. 193.

[15] Ghafoori, M., A. Rastegarnia, and G.R. Lashkaripour, Estimation of static parameters based on dynamical and physical properties in limestone rocks. Journal of African Earth Sciences, 2018. 137: p. 22-31.

[16] Tariq, Z., S. Elkatatny, M. Mahmoud, and A. Abdulraheem. A holistic approach to develop new rigorous empirical correlation for static Young's modulus. in Abu Dhabi International Petroleum Exhibition & Conference. 2016. Society of Petroleum Engineers.

[17] Brotons, V., et al., Improved correlation between the static and dynamic elastic modulus of different types of rocks. Materials and structures, 2016. 49(8): p. 3021-3037.

[18] Fjær, E., Relations between static and dynamic moduli of sedimentary rocks .Geophysical Prospecting, 2019. 67(1): p. 128-139.

[19] He, J., et al. Static and Dynamic Elastic Moduli of Bakken Formation. in International Petroleum Technology Conference. 2019. International Petroleum Technology Conference.

[20] Martínez-Martínez, J .,D. Benavente, and M. García-del-Cura, Comparison of the static and dynamic elastic modulus in carbonate rocks. Bulletin of engineering geology and the environment, 2012. 71(2): p. 263-268.

[21] Missagia, R.M., L. Oliveira, I.D.A.L. Neto, and M.R. de Ceia .Evaluation of Static and Dynamic Elastic Properties in Carbonate Rocks. in 81st EAGE Conference and Exhibition 2019. 2019.

[22] Rashidi, M., M. Hajipour, and A. Asadi. Correlation Between Static and Dynamic Elastic Modulus of Limestone Formations Using Artificial Neural Networks. in 52nd US Rock Mechanics/Geomechanics Symposium. 2018. American Rock Mechanics Association.

[23] Pourrostam, A., Estimation of Porosity and Permeability Parameters Using Well-Log and Core Data from a Gas Field in South of Iran, in Faculty of science, Department of physics. 2016, Razi University.

[24] Mehrgini, B., et al., Geomechanical characterization of a south Iran carbonate reservoir rock at ambient and reservoir temperatures. Journal of Natural Gas Science and Engineering, 2016 **:٣٤** .p. 269-279.

[25] Nur, A.M. and Z. Wang, Seismic and Acoustic Velocities in Reservoir Rocks: Recent Developments Vol. 3 : Recent Developments. 2000, United States: American Association of Petroleum Geologists.

[26] Kılıç, A. and A. Teymen, Determination of mechanical properties of rocks using simple methods. Bulletin of Engineering Geology and the Environment, 2008. 67(2): p. 237.

[27] Aboutaleb, S., R. Bagherpour, M. Behnia, and M. Aghababaei, Combination of the physical and ultrasonic tests in estimating the uniaxial compressive strength and Young's modulus of intact limestone rocks. Geotechnical and Geological Engineering, 2017. 35(6): p. 3015-3023.

[28] Eissa, E. and A. Kazi, Relation between static and dynamic Young's moduli of rocks. International Journal of Rock Mechanics and Mining & Geomechanics Abstracts, 1988. 25.**(٦)**

[29] Dinçer, İ., A. Acar, and S. Ural, Estimation of strength and deformation properties of Quaternary caliche deposits. Bulletin of Engineering Geology and the Environment, 2008. 67 **:(٣)**p. 353-366.

[30] Torabi-Kaveh, M., F. Naseri, S. Saneie, and B. Sarshari, Application of artificial neural networks and multivariate statistics to predict UCS and E using physical properties of Asmari limestones. Arabian journal of Geosciences, 2015 **:(٥)٨** .p. 2889-2897.

[31] Anemangely, M., A. Ramezanzadeh, and M.M. Behboud, Geomechanical parameter estimation from mechanical specific energy using artificial intelligence. Journal of Petroleum Science and Engineering, 2019. 175: p. 407-429.

[32] Asef, M .and M. Farrokhrouz, Governing parameters for approximation of carbonates UCS. Electron J Geotech Eng, 2010. 15: p. 1581-1592.

[33] Minaeian, B. and K. Ahangari, Estimation of uniaxial compressive strength based on P-wave and Schmidt hammer rebound using statistical method. Arabian Journal of Geosciences, 2013. 6(6): p. 1925-1931.

[34] Nourani Asl, R., Estimation of uniaxial compressive strength and young's modulus of intact rocks using the multiple statistic methods, in Department of Mining Engineering. 200 ,Tarbiat Modares University: Tehran, Iran.

[35] Golubev, A. and G. Rabinovich, Resultaty primeneia appartury akusticeskogo karotasa dlja predeleina proconstych svoistv gornych porod na mestorosdeniaach tverdych isjopaemych. Prikl. Geofiz. Moskva, 1976. 7 :۳p. 109-116.

[36] Moradian, Z. and M. Behnia, Predicting the uniaxial compressive strength and static Young's modulus of intact sedimentary rocks using the ultrasonic test. International Journal of Geomechanics, 2009. 9(1): p. 14-19.

[37] Eberhart, R. and J. Kennedy. Particle swarm optimization. in Proceedings of the IEEE international conference on neural networks. 1995. Citeseer.

[38] Anemangely, M., A. Ramezanzadeh, and B. Tokhmechi, Shear wave travel time estimation from petrophysical logs using ANFIS-PSO algorithm: A case study from Ab-Teymour Oilfield. Journal of Natural Gas Science and Engineering, 2017. 38: p. 373-387.

[39] Anemangely, M., A. Ramezanzadeh, and B. Tokhmechi, Determination of constant coefficients of Bourgoyne and Young drilling rate model using a novel evolutionary algorithm. Journal of Mining and Environment, 2017. 8(4): p. 693-702.

[40] Anemangely, M., A. Ramezanzadeh, H. Amiri, and S.-A. Hoseinpour, Machine learning technique for the prediction of shear wave velocity using petrophysical logs. Journal of Petroleum Science and Engineering, 2019. 174: p. 306-327.

[41] Anemangely, M., A. Ramezanzadeh, and M. Mohammadi Behboud, Geomechanical parameter estimation from mechanical specific energy using artificial intelligence. Journal of Petroleum Science and Engineering, 2019. 175: p. 407-429.

[42] Anemangely, M., et al., Drilling rate prediction from petrophysical logs and mud logging data using an optimized multilayer perceptron neural network. Journal of Geophysics and Engineering, 201: p. 1146-1159.

[43] Anemangely, M., et al., Development of a new rock drillability index for oil and gas reservoir rocks using punch penetration test. Journal of Petroleum Science and Engineering, 2018. 166: p. 131-145.

[44] Sabah, M., et al., A machine learning approach to predict drilling rate using petrophysical and mud logging data. Earth Science Informatics, 2019: p. 1-21.

[45] Pedersen, M.E.H. and A.J. Chipperfield, Simplifying Particle Swarm Optimization. Applied Soft Computing, 2010. 10(2): p. 618-628.

[46] Coello, C.A.C., G.B. Lamont, and D.A. Van Veldhuizen, Evolutionary algorithms for solving multi-objective problems. Vol. 5. 2007: Springer.

[47] Maity, R., Statistical methods in hydrology and hydroclimatology. 2018: Springer.

[48] Brotons, V ,.R. Tomás, S. Ivorra, and A. Grediaga, Relationship between static and dynamic elastic modulus of calcarenite heated at different temperatures: the San Julián's stone. Bulletin of Engineering Geology and the Environment, 2014. 73(3): p. 791-799.

[49] Christaras, B., F. Auger, and E. Mosse, Determination of the moduli of elasticity of rocks. Comparison of the ultrasonic velocity and mechanical resonance frequency methods with direct static methods. Materials and Structures, 1994. 27(4): p. 222-228.

[50] Ameen, M.S., et al., Predicting rock mechanical properties of carbonates from wireline logs (A case study: Arab-D reservoir, Ghawar field, Saudi Arabia). Marine and Petroleum Geology, 2009. 26(4): p. 430-444.

[51] Lacy, L.L. Dynamic rock mechanics testing for optimized fracture designs. in SPE annual technical conference and exhibition. 1997. Society of Petroleum Engineers.

[52] KIANPOUR, M., M. SAYARI, and A. OROMIEHIE, A FUZZY MODEL TO PREDICT THE UNIAXIAL COMPRESSIVE STRENGTH AND THE MODULUS OF ELASTICITY OF SHEMSHAK FORMATION SHALES. Geol Mag, 2012(83): p. 103–110.

[53] Yilmaz, I. and A. Yuksek, An example of artificial neural network (ANN) application for indirect estimation of rock parameters. Rock mechanics and rock engineering, 2008. 41(5): p. 781.

[54] Yasar, E. and Y. Erdogan, Correlating sound velocity with the density, compressive strength and Young's modulus of carbonate rocks. International Journal of Rock Mechanics and Mining Sciences, 2004. 41(5): p. 871-875.

[55] Horsrud, P., Estimating mechanical properties of shale from empirical correlations. SPE Drilling & Completion, 2001. 16(02): p. 68-73.

[56] Rzhevsky, V. and G. Novik, The Physics of rocks. 320 str. Mir Publischers. Moskva, 1971.

[57] Lashkaripour, G.R., Predicting mechanical properties of mudrock from index parameters. Bulletin of Engineering Geology and the Environment, 2002. 61(1): p. 73-77.

[58] Lashkaripour GR, D.M., Prediction mechanical properties of mud rock from index parameters, in Conference on Probabilistic Methods in Geotechnical Engineering. 1993: Australia,. p. 195–200.

[59] Vernik, L., M. Bruno, and C. Bovberg. Empirical relations between compressive strength and porosity of siliciclastic rocks. in International journal of rock mechanics and mining sciences & geomechanics abstracts. 1993. Elsevier.

[60] Dehghan, S., G. Sattari, S.C. Chelgani, and M. Aliabadi, Prediction of uniaxial compressive strength and modulus of elasticity for Travertine samples using regression and artificial neural networks. Mining Science and Technology (China), 2010. 20(1): p. 41-46.

[61] Yilmaz, I., Prediction of the strength and elasticity modulus of gypsum using multiple regression, ANN, and ANFIS models. Int. J. Rock Mech. Min. Sci., 2009. 46: p. 803-810.

[62] Garagon, M. and T. Çan, Predicting the strength anisotropy in uniaxial compression of some laminated sandstones using multivariate regression analysis. Materials and structures, 2010. 43(4): p. 509-517.

[63] Bradford, I., J. Fuller, P. Thompson, and T. Walsgrove. Benefits of assessing the solids production risk in a North Sea reservoir using elastoplastic modelling. in SPE/ISRM Rock Mechanics in Petroleum Engineering. 1998. Society of Petroleum Engineers.

[64] Soroush, H., Evaluation of moisture effect on mechanical properties and determination of effective quantitative indexes, in Department of Mining and Metals. 1998, Amirkabir University of Technology: Tehran, Iran.

[65] Karakul, H. and R. Ulusay, Empirical correlations for predicting strength properties of rocks from P-wave velocity under different degrees of saturation. Rock mechanics and rock engineering, 2013. 46(5): p. 981-999.

[66] Selçuk, L. and A. Nar, Prediction of uniaxial compressive strength of intact rocks using ultrasonic pulse velocity and rebound-hammer number. Quarterly Journal of Engineering Geology and Hydrogeology, 2016. 49(1): p. 67-75.

[67] Altindag, R., Correlation between P-wave velocity and some mechanical properties for sedimentary rocks. Journal of the Southern African Institute of Mining and Metallurgy, 2012. 112(3): . 229-237.

[68] Beiki, M., A. Majdi, and A.D. Givshad, Application of genetic programming to predict the uniaxial compressive strength and elastic modulus of carbonate rocks. International Journal of Rock Mechanics and Mining Sciences, 2013(63): p. 159-169.

[69] Kahraman, S., Evaluation of simple methods for assessing the uniaxial compressive strength of rock. International Journal of Rock Mechanics and Mining Sciences, 2001. 38(7): p. 981-994.

[70] Mohamad, E.T., D.J. Armaghani, E. Momeni, and S.V.A.N.K. Abad, Prediction of the unconfined compressive strength of soft rocks: a PSO-based ANN approach. Bulletin of Engineering Geology and the Environment, 2015. 74(3): p. 745-757.

[71] Çobanoğlu, İ. and S.B. Çelik, Estimation of uniaxial compressive strength from point load strength, Schmidt hardness and P-wave velocity. Bulletin of Engineering Geology and the Environment, 2008. 67(4): p. 491-498.

[72] Ghazvinian, A., V. Rasouli, and R. Nourani Asl. Application of multiple statistic methods in estimation of uniaxial compressive strength of intact rocks using indirect tests. in Proceedings of 3rd Rock Mech Congress, Tehran, Iran. 2007.

[73] Azimian, A., Application of statistical methods for predicting uniaxial compressive strength of limestone rocks using nondestructive tests. Acta Geotechnica, 2017. 12(2): p. 321-333.

[74] Hakan, E. and D. Kanik, Multicriteria decision-making analysis based methodology for predicting carbonate rocks' uniaxial compressive strength. Earth Sciences Research Journal, 2012. 16(1): p. 65.٧٤-

[75] Khandelwal, M., Correlating P-wave velocity with the physico-mechanical properties of different rocks. Pure and Applied Geophysics, 2013. 170(4): p. 507-514.

[76] Militzer, H., Einige Beiträge der Geophysik zur primärdatenerfassung im Bergbau. 1973.

[77] Kurtuluş, C., F. Sertçelik, and I. Sertçelik, Correlating physico-mechanical properties of intact

rocks with P-wave velocity. Acta Geodaetica et Geophysica, 2016. 51(3): p. 571-582**.**

[78] Freyburg, E., Der Untere und mittlere Buntsandstein SW-Thuringen in seinen gesteinstechnicschen Eigenschaften. Deustche Gesellschaft Geologische Wissenschaften. A; Berlin, 1972. 176: p. 911-919**.**

[79] Sharma, P. and T. Singh, A correlation between P-wave velocity, impact strength index, slake durability index and uniaxial compressive strength. Bulletin of Engineering Geology and the Environment, 2008. 67(1): p. 17-22**.**

[80] Shalabi, F.I., E.J. Cording, and O.H. Al-Hattamleh, Estimation of rock engineering properties using hardness tests. Engineering Geology, 2007. 90 p. 138-147**.**

[81] Moos, D., P. Peska, T. Finkbeiner, and M. Zoback, Comprehensive wellbore stability analysis utilizing quantitative risk assessment. Journal of Petroleum Science and Engineering, 2003. 38(3-4): p. 97-109.

[82] Ceryan, N., U. Okkan, and A **.**Kesimal, Prediction of unconfined compressive strength of carbonate rocks using artificial neural networks. Environmental earth sciences, 2013. 68(3): p. 807-819**.**

Appendix I. Evaluation of the existing correlations for estimating the Esta and UCS of carbonate rocks in the literature

Table 9. Correlations presented for estimating the E_{sta} of carbonate rocks based on physical parameters of the rock including the porosity, *n*, the density, ρ, the compressive wave velocity, V_p, the shear wave velocity, V_s, and the dynamic Young's modulus, E_{dyn}.

Input parameter(s)	References	Equation for E_s estimation	RMSE (GPa)	R-squared
E_{dyn}	[25]	$E_{sta} = 1.153E_d - 15.2$	3.12	0.86
	[48]	$E_{sta} = 0.867E_d - 2.085$	5.49	0.85
	[28]	$E_{sta} = 0.74E_d - 0.82$	6.54	0.85
	[31]	$E_{sta} = 0.70E_d$	7.09	0.85
	[49]	$E_{sta} = 1.05E_d - 3.16$	7.58	0.85
	[6]	$E_{sta} = 0.14E_d^{1.96}$	9.40	0.86
	[50]	$E_{sta} = 0.541E_d + 12.852$	11.85	0.85
	[51]	$E_{sta} = 0.018E_d^2 + 0.422E_d$	14.30	0.86
n	[24]	$E_{sta} = 69 - 19.3 \ln(n)$	5.89	0.89
	[52]	$E_{sta} = 12.16 - 1.532n$	19.58	0.82
	[34]	$E_{sta} = 69 - 19.3 \ln(n)$	22.31	0.83
	[34]	$E_{sta} = 7.39 - 0.21n$	23.32	0.82
	[53]	$E_{sta} = 6.7396 + 2.6715n$	47.28	0.82
Vp	[6]	$E_{sta} = 0.169V_p^{3.324}$	9.81	0.94
	[54]	$E_{sta} = 10.672V_p - 18.706$	10.21	0.92
	[55]	$E_{sta} = 0.076 \times V_p^{3.23}$	20.53	0.94
	[34]	$E_{sta} = V_p - 1.41$	25.40	0.92
ρ	[29]	$E_{sta} = 3.98 \times e^{5.238\rho}$	23.65	0.86
ρ, E_d	[28]	$E_{sta} = 10^{(0.02+0.7\log(\rho E_{dyn}))}$	8.05	0.87
ρ, n, V_p	[30]	$E_{sta} = 76.534 - 2.709\rho + 0.271n - 11V_p$	29.52	0.93
	[30]	$E_{sta} = 71.712 - 0.154\rho^3 + 0.002n^3 - 10V_p$	44.21	0.73
, n, Vp, Vsρ	[27]	$E_{sta} = -23.689 + 2.99\rho - 0.36n + 19.835V_p - 19V_s$	13.48	0.89

E_s, E_d: (GPa), Vp, Vs: (km/s), ρ: (g/cc), n: (%)

Table 10. Correlations presented for estimating the UCS of carbonate rocks based on physical parameters of the rock including the porosity, *n*, the density, ρ, the compressive wave velocity, V_p, and the shear wave velocity, V_s.

Input Parameter(s)	Researcher (Year)	Equation for UCS estimation	RMSE (MPa)	R-squared
n	[26]	$UCS = 147.16 \times e^{-0.0835n}$	15.15	0.90
	[24]	$UCS = -48 \times \ln(n) + 174$	15.60	0.89
	[56]	$UCS = 143.8 \times e^{-6.95n}$	17.57	0.89
	[57]	$UCS = 210.12 \times n^{-0.821}$	26.70	0.75
	[56]	$UCS = 135.9 \times e^{-4.8n}$	26.90	0.87
	[55]	$UCS = 2.922 \times n^{-0.96}$	30.52	0.71
	[55]	$UCS = 0.77 \times V_p^{2.93}$	31.09	0.77
	[34]	$UCS = 72.3 - 2.22n$	33.63	0.79
	[58]	$UCS = 1.001 \times n^{-1.143}$	40.30	0.66
	[52]	$UCS = 76.107 \times e^{-0.4153n}$	46.53	0.79
	[59]	$UCS = 277 \times e^{-10n}$	48.80	0.91
	[60]	$UCS = 35.722 - 0.451n$	49.56	0.79
	[61]	$UCS = 78.989 - 28.429 \ln(n)$	49.74	0.89
	[29]	$UCS = 42.111 \times e^{-0.083n}$	52.73	0.90
	[62]	$UCS = 46.402 \times e^{-0.138n}$	55.32	0.90

	[52]	$UCS = 79.9 - 32\ln(n)$	55.77	0.89
	[29]	$UCS = 16.717 - 0.439n$	61.60	0.79
	[63]	$UCS = 254 \times (1 - 2.7n)^2$	61.79	0.86
	[56]	$UCS = 276 \times (1 - 3n)^2$	65.86	0.88
	[53]	$UCS = 3.1096 + 2.332n$	67.17	0.79
	[29]	$UCS = -10.96\ln(n) - 40.826$	80.29	0.89
	[64]	$UCS = 101.3 - 31.4\ln(n)$	117.41	0.89
Vp	[33]	$UCS = e^{0.99V_p}$	23.49	0.74
	[26]	$UCS = 2.304 \times V_p^{2.4315}$	25.78	0.78
	[35]	$UCS = 10^{0.358V_p} + 0.283$	26.34	0.75
	[6]	$UCS = 0.009V_p^{1.105}$	27.93	0.78
	[54]	$UCS = 31.545V_p - 63.706$	28.60	0.77
	[65]	$UCS = 7.182V_p^{1.6}$	31.64	0.78
	[53]	$UCS = 3.9348 \times e^{0.6129V_p}$	31.77	0.77
	[66]	$UCS = 22.18V_p - 30.32$	33.17	0.77
	[67]	$UCS = 12.743V_p^{1.194}$	35.16	0.77
	[68]	$UCS = 3.7V_p^{2.3}$	35.26	0.78
	[69]	$UCS = 9.95 \times V_p^{1.21}$	36.77	0.77
	[36]	$UCS = 165.05 \times e^{-4.452/V_p}$	37.24	0.76
	[70]	$UCS = 33V_p - 44.227$	37.70	0.77
	[71]	$UCS = 56.71V_p - 192.93$	40.51	0.77
	[72]	$UCS = 16.4V_p - 16.42$	40.62	0.77
	[73]	$UCS = 0.009V_p^{1.105}$	41.38	0.77
	[74]	$UCS = 15\ln(V_p) - 73^a$	43.72	0.76
	[75]	$UCS = 33V_p - 34.83$	44.47	0.77
	[76]	$UCS = 2.45V_p^{1.82}$	46.20	0.78
	[74]	$UCS = 0.0009V_p\,[m/s] + 38^a$	47.21	0.77
	[77]	$UCS = 8.10^{-6}V_p^2 - 0.024V_p + 31.92$	51.27	0.77
	[29]	$UCS = 6.97 \times V_p^{0.963}$	51.51	0.77
	[34]	$UCS = 10V_p - 16.42$	52.12	0.77
	[78]	$UCS = 0.035V_p - 31.5$	53.01	0.77
	[29]	$UCS = 6V_p - 0.556$	53.44	0.77
	[33]	$UCS = 5V_p$	55.93	0.77
	[29]	$UCS = 7.141 + 5.136\ln(V_p)$	60.87	0.76
	[33]	$UCS = 16.074 + 2.327\ln(V_p)$	70.68	0.76
	[33]	$UCS = 1.016 \times V_p^{0.0023}$	70.68	0.76
	[79]	$UCS = 64.2V_p - 117.99$	72.63	0.77
	[29]	$UCS = 2.054 \times e^{V_p}$	81.97	0.74
ρ	[34]	$UCS = 70.74\,\rho_{dry} - 116.26$	29.27	0.79
	[80]	$UCS = 73\rho - 110.32$	29.51	0.79
	[62]	$UCS = 0.632 \times 10^{-4} \times \rho^{14.5}$	38.16	0.78
	[29]	$UCS = 0.0737 \times e^{2.17\rho}$	54.31	0.86
	[29]	$UCS = 0.33 \times \rho^{4.108}$	58.45	0.84
	[29]	$UCS = 11.31\rho - 16.47$	61.86	0.79
	[29]	$UCS = 21.035\ln(\rho) - 8.375$	62.82	0.76
***ρ*, Vp**	[36]	$UCS = 142.47 \times e^{-9.561/(\rho V_p)}$	33.75	0.80

	[81]	$UCS = 4.21 \times e^{(1.9\times10^{-11}\rho V_p^2)}$	47.54	0.82
	[29]	$UCS = -6.319 + 4.27\rho + 4.418V_p$	54.34	0.81
	[81]	$UCS = 3.87 \times e^{(1.14\times10^{-10}\rho V_p^2)}$	68.53	0.82
	[14]	$UCS = 29.3\rho\ [\mathrm{kN/m^3})\ ] + 0.4V_p - 687.43^b$	70.35	0.79
	[81]	$UCS = 1.745 \times 10^{-9}\rho V_p^2 - 21$	88.61	0.82
$\boldsymbol{n, V_p}$	[82]	$UCS = 5.77 - 0.132n + 2.25V_p$	60.80	0.82
$\boldsymbol{\rho, n, V_p}$	[27]	$UCS = -92.305 + 33.66\rho - 0.61n + 12.27V_p + 3V_s$	35.10	0.83
$\boldsymbol{E_{sta}}$, **n**	[32]	$UCS = 2.94 \times {E_{sta}}^{0.834}/n^{0.088}$	19.35	0.87
$\boldsymbol{E_{sta}}$	[31]	$UCS = 2.27E_{sta} + 4.74$	17.77	0.86
	[35]	$UCS = 25.1 \times {E_{sta}}^{0.34}$	32.15	0.84
	[35]	$UCS = 13.8 \times {E_{sta}}^{0.51}$	28.54	0.86
$\boldsymbol{E_{dyn}}$	[6]	$UCS = 12.8 \times (E_{dyn}/10)^{1.32}$	18.02	0.86

UCS: (MPa), Vp, Vs: (km/s), ρ: (g/cc)

Appendix II. Development of estimator models for Esta and UCS using the PSO algorithm and RA

Table 11. The models developed for estimating the E_{sta} using the PSO algorithm based on the studied data.

Input parameter	Eq. Type	Equation	RMSE (GPa)	R-squared
V_s	Exponential	$E_{sta} = 0.3098e^{1.8103V_s}$	3.30	0.96
	Power	$E_{sta} = 0.5284V_s^{4.4033}$	3.60	0.96
	Linear	$E_{sta} = 36.8831V_s - 58.642$	6.21	0.87
V_p	Exponential	$E_{sta} = 0.5191e^{0.9354V_p}$	4.43	0.93
	Power	$E_{sta} = 0.0952V_p^{3.9546}$	4.14	0.94
	Linear	$E_{sta} = 23.5739V_p - 67.0820$	4.94	0.92
ρ	Exponential	$E_{sta} = 0.0332e^{2.6215\rho}$	5.28	0.90
	Power	$E_{sta} = 0.0551\rho^{6.6289}$	5.34	0.90
	Linear	$E_{sta} = 52.7608\rho - 102.9819$	7.13	0.83
n	Exponential	$E_{sta} = 61.1913e^{-0.893n}$	5.22	0.91
	Power	$E_{sta} = 72.7183n^{-0.5512}$	7.61	0.81
	Linear	$E_{sta} = -1.7174n + 47.5796$	7.30	0.82
E_{dyn}	Exponential	$E_{sta} = 4.9280e^{0.0425E_{dyn}}$	3.07	0.97
	Power	$E_{sta} = 0.0691E_{dyn}^{1.6505}$	2.11	0.98
	Linear	$E_{sta} = 1.1194E_{dyn} - 12.0313$	3.25	0.96

Table 12. The models developed for estimating the UCS using the PSO algorithm based on the studied data.

Input Parameter(s)	Eq. Type	Equation	RMSE (MPa)	R-squared
E_{dyn}	Exponential	$UCS = 13.3257e^{0.0410E_{dyn}}$	19.02	0.83
	Power	$UCS = 0.2111E_{dyn}^{1.6006}$	16.92	0.86
	Linear	$UCS = 2.8315E_{dyn} - 30.6291$	17.44	0.86
E_{sta}	Exponential	$UCS = 25.8185e^{0.0296E_{sta}}$	23.21	0.75
	Power	$UCS = 3.0347E_{sta}^{0.9484}$	17.29	0.86
	Linear	$UCS = 2.4845E_{sta} + 0.7796$	17.38	0.86
n	Exponential	$UCS = 164.5985e^{-0.0979n}$	14.11	0.91
	Power	$UCS = 194.1561n^{-0.5806}$	20.22	0.81
	Linear	$UCS = -4.5222n + 122.8295$	21.22	0.79
ρ	Exponential	$UCS = 0.0771e^{2.6559\rho}$	17.50	0.85
	Power	$UCS = 0.1218\rho^{6.7751}$	17.33	0.86
	Linear	$UCS = 138.3005\rho - 272.1419$	21.17	0.79
V_p	Exponential	$UCS = 1.7206e^{0.8725V_p}$	23.01	0.75
	Power	$UCS = 0.3573V_p^{3.6834}$	22.27	0.76
	Linear	$UCS = 58.0776V_p - 164.0326$	21.91	0.77
V_s	Exponential	$UCS = 0.8356e^{1.7852V_s}$	17.78	0.85
	Power	$UCS = 1.4115V_s^{4.3454}$	17.93	0.85
	Linear	$UCS = 93.7004V_s - 149.4189$	21.66	0.78
V_p, ρ	Exponential	$UCS = 1000 \times e^{-28.7/(\rho^{1.8316}\, V_p{}^{0.4825})}$	16.11	0.88
V_p, ρ, n	Exponential Power	$UCS = 259.9612 \times n^{-0.25} \times e^{-68.7524\rho^{-3.0119}V_p^{-1.1706}}$	14.69	0.90

Table 13. The models developed for estimating the E_{sta} using the RA based on the studied data.

Parameter	Eq. Type	Equation	RMSE (GPa)	R-squared
V_s	Exponential	$E_{sta} = 0.3372e^{1.7695V_s}$	3.38	0.91
	Power	$E_{sta} = 0.8694V_s^{3.8302}$	4.26	0.90
	Linear	$E_{sta} = 36.883V_s - 58.642$	6.21	0.87
V_p	Exponential	$E_{sta} = 0.249e^{1.1039V_p}$	5.36	0.92
	Power	$E_{sta} = 0.0567V_p^{4.3034}$	4.34	0.93
	Linear	$E_{sta} = 23.574V_p - 67.082$	4.94	0.92
ρ	Exponential	$E_{sta} = 0.0339e^{2.6036\rho}$	5.32	0.92
	Power	$E_{sta} = 0.0853\rho^{6.13.48}$	5.58	0.92
	Linear	$E_{sta} = 52.761\rho - 102.98$	7.13	0.83
n	Exponential	$E_{sta} = 57.293e^{-0.085n}$	5.38	0.92
	Power	$E_{sta} = 106.22n^{-0.788}$	10.80	0.83
	Linear	$E_{sta} = -1.717n + 47.58$	7.30	0.82
E_{dyn}	Exponential	$E_{sta} = 3.3508e^{0.0517E_{dyn}}$	5.04	0.94
	Power	$E_{sta} = 0.0893E_{dyn}^{1.5785}$	2.26	0.96
	Linear	$E_{sta} = 1.1194E_{dyn} - 12.031$	3.25	0.96

Table 14. The models developed for estimating the UCS using the RA based on the studied data.

Input Parameter	Eq. Type	Equation	RMSE (MPa)	R-squared
E_{dyn}	Exponential	$UCS = 7.9205e^{0.0526E_{dyn}}$	22.32	0.87
	Power	$UCS = 0.2009E_{dyn}^{1.6017}$	17.20	0.88
	Linear	$UCS = 2.8315E_{dyn} - 30.629$	17.44	0.86
E_{sta}	Exponential	$UCS = 14.566e^{0.045E_{sta}}$	33.81	0.83
	Power	$UCS = 2.3148E_{sta}^{1.0171}$	17.49	0.92
	Linear	$UCS = 2.4845E_{sta} + 0.7796$	17.38	0.86
n	Exponential	$UCS = 144.27e^{-0.087n}$	15.46	0.87
	Power	$UCS = 284.43n^{-0.829}$	28.64	0.82
	Linear	$UCS = -4.522 + 122.83$	21.22	0.79
ρ	Exponential	$UCS = 0.064e^{2.7093\rho}$	17.75	0.89
	Power	$UCS = 0.1693\rho^{6.371}$	18.06	0.88
	Linear	$UCS = 138.3\rho - 272.14$	21.17	0.79
V_p	Exponential	$UCS = 0.5835e^{1.1133V_p}$	25.06	0.84
	Power	$UCS = 0.1284V_p^{4.3569}$	23.06	0.85
	Linear	$UCS = 58.078V_p - 164.03$	21.91	0.77
V_s	Exponential	$UCS = 0.7911e^{1.785V_s}$	18.16	0.83
	Power	$UCS = 2.0724V_s^{3.8539}$	19.33	0.81
	Linear	$UCS = 93.7V_s - 149.42$	21.66	0.78